Rheol Acta (2015) 54:109–119
DOI 10.1007/s00397-014-0828-5

ORIGINAL CONTRIBUTION

Fractional modelling of functionalized CNT suspensions

Jose Vicente Aguado · Emmanuelle Abisset-Chavanne · Elias Cueto · Francisco Chinesta · Roland Keunings

Received: 1 July 2014 / Revised: 6 November 2014 / Accepted: 21 November 2014 / Published online: 10 December 2014

Abstract Experimental findings and rheological modelling of chemically treated single-wall carbon nanotubes suspended in an epoxy resin were addressed in a recent publication (Ma et al., J Rheol 53:547–573, 2009). The shear-thinning behaviour was successfully modelled by a Fokker-Planck-based orientation model. However, the proposed model failed to describe linear viscoelasticity using a single mode as well as the relaxation after applying a finite step strain. Both experiments revealed a power-law behaviour for the storage and relaxation moduli. In this paper, we show that a single-mode fractional diffusion model is able to predict these experimental observations.

Keywords Fractional derivatives · Functionalized CNTs · Small-amplitude oscillatory flows · Linear viscoelasticity

J. V. Aguado · E. Abisset-Chavanne · F. Chinesta (✉)
GeM, UMR CNRS-Centrale Nantes, 1 rue de la Noe,
BP 92101, 44321 Nantes Cedex 3, France
e-mail: francisco.chinesta@ec-nantes.fr

J. V. Aguado
e-mail: jose.aguado-lopez@ec-nantes.fr

E. Cueto
I3A, Aragon Institute of Engineering Research,
Universidad de Zaragoza, Maria de Luna s/n,
Zaragoza, Spain

R. Keunings
ICTEAM, Université Catholique de Louvain,
Bat. Euler, Av. Georges Lemaitre 4,
1348 Louvain-la-Neuve, Belgium

Introduction

The rheological modelling of untreated and chemically treated carbon nanotubes (CNTs) suspended in an epoxy resin was addressed in Ma et al. (2008). The resulting models were applied to simulate complex flows (Cueto et al. 2008; 2010).

The untreated CNT suspensions exhibited significant shear-thinning behaviour in a steady-state simple shear flow and contained optically resolvable aggregate structures depending on the applied shear rate (Ma et al. 2008). A simple orientation model, based on a Fokker-Planck advection-diffusion description, failed to capture the experimentally observed rheological responses for untreated CNT suspensions. A new model named the 'aggregation/orientation' (AO) model was then developed to describe the experimental findings (Ma et al. 2008). A hierarchy of states between CNTs that are free from entanglement and a complete CNT network were incorporated into the AO model, thereby enabling different microstructure populations to exist for different shear conditions. Using a small number of adjustable parameters, it was found that the experimental data could be fitted with reasonable accuracy. A comparison between the rheology of CNTs and carbon black suspensions was carried out in Yearsley et al. (2012). These studies motivated our recent works on the modelling and simulation of CNT aggregates (Abisset-Chavanne et al. 2013; 2014).

In the case of chemically treated CNTs suspended in an epoxy resin, the aggregation is prevented and we can consider that we are dealing with a large population of free rods in the diluted regime or rods experiencing interactions in the semi-concentrated or concentrated regimes. Thus, when a suspension of functionalized CNTs was subject to a steady-state shear flow, it exhibited a shear-thinning behaviour, which was subsequently modelled by a

Fokker-Planck (FP)-based orientation model (Ma et al. 2009). The model assumes that the shear flow aligns the CNTs in the flow direction, but there are events such as Brownian motion and tube-tube interactions that randomize the orientation. In the FP-based orientation model, randomizing events were modelled with an appropriate rotary diffusion coefficient (D_r) and the shear-thinning behaviour was explained in terms of progressive alignment of CNTs towards the shear direction.

With regard to linear viscoelasticity (LVE), small-amplitude oscillatory measurements revealed mild elasticity for semi-diluted, treated CNT suspensions. The exact origin for this elasticity is not clear, and both tube-tube interactions and bending/stretching of CNTs have been proposed by other authors as possible origins (see Cruz et al. (2010) and the references therein).

Intuitively, chemical treatment creates a weakly interconnected network of CNTs and it is believed that the mild elasticity originates from this weak network as well as other randomizing events (Brownian motion and tube-tube hydrodynamic interactions). Step strain experiments confirmed the presence of a weak network at small strains, which was found to be destroyed at large strains.

Brownian dynamics modelling was addressed in Cruz et al. (2010) and (2012), where the elasticity effects were explained as a direct consequence of the bending of CNTs having a non-straight natural configuration due to side-wall defects.

Experimental LVE data of the treated CNT suspensions were fitted in Ma et al. (2009) using the FP-based orientation model with an effective diffusion coefficient term. An empirical relation was subsequently identified for the effective diffusion term that assumed a dependency of the diffusion coefficient on the applied frequency in order to avoid the introduction of a large number of mechanisms that are difficult to support on physical grounds.

It should be noticed, however, that such an approach based on the use of a single mode and a diffusion coefficient depending on the applied frequency is inconsistent. Indeed, we firstly assumed linearity, i.e. a diffusion coefficient independent on the applied frequency. Then, in order to fit the experimental results, the diffusion coefficient was assumed to be dependent on the applied frequency. Thus, from a linear assumption, we concluded on a non-linear behaviour that invalidated the analysis carried out. Concerning the relaxation after applying a finite step strain, the model presented in Ma et al. (2009) was unable to describe the experimental results that again exhibit a power-law evolution instead of the exponential one that the proposed model predicted.

In this paper, we revisit the experimental results reported in Ma et al. (2009) concerning chemically treated CNTs, in particular those related to LVE and step strain relaxation after applying a finite step strain. We show that a fractional diffusion model with a single mode is only able to predict the power-law behaviour observed in both experiments.

Experimental details

In what follows, we briefly summarize the experiments carried out by Ma and Mackley in Cambridge, whose results were reported in Ma et al. (2009).

Single-walled CNTs were produced by high-pressure carbon monoxide disproportionation that were supplied by Nanocomposites Inc., USA. In the case of treated CNTs, aggregation was prevented by covalently attaching arene-diazonium salts onto the sidewall of CNTs. The treated CNT suspensions were stabilized via electrostatic repulsion between CNTs.

Microstructure of resulting mixtures was optically characterized using the Cambridge Shear System. Optical analysis proved that the suspension showed no optically resolvable aggregates of CNTs, and the mixture was well dispersed at the micron level. By contrast, the untreated CNT suspension consisted of optically resolvable CNT aggregates (Rahatekar et al. 2006).

Rheological measurements were made using an ARES strain-controlled rheometer with 50-mm parallel plates and a gap size of 0.3 mm. In the small-amplitude oscillatory shear experiment, a strain amplitude of 1 % was used. In order to minimize the possible complication from sample loading, samples were slowly squeezed between the parallel plates and were rested for at least 2 h before any measurements were carried out. Step strain experiments were carried out in order to explore the transition from small to large strain deformations.

LVE of CNT suspensions was studied using small-amplitude oscillatory measurements. Epoxy resin showed the scattered G' data with torque values very close to the detection limit of the transducer, implying that the elasticity of the matrix is negligible ($G'_{\text{epoxy}} \approx 0$). Epoxy behaved essentially as a Newtonian fluid with viscous dissipation that is consistent with steady shear measurements. Addition of CNTs increased the values of both G' and G'' as reported in Ma et al. (2009). Measurements were made at a strain of 1 %, which was well within the linear strain response of the suspensions. The enhancement of G' was concentration dependent and more pronounced at high concentration levels (0.2 and 0.5 %). The evolution of G' as a function of frequency is consistent with experimental results reported by Song and Youn (2005) and Xu et al. (2005). The addition of CNTs increased the elasticity of the system as a whole (Ma et al. 2009). This response is very different from that of a typical short-fibre suspension, where the addition of fibres was reported to have no extra contribution to the

storage modulus (G') of the suspending medium (Carter 1967; Ganani and Powell 1986).

To assess the relative importance of viscous and elastic contributions at a given concentration, we show in Fig. 1 the obtained data for G', G'' and η^* for the 0.5 % CNT suspension. The value of G'' was observed to be higher than that of G' within the full range of frequency studied, which implies that the elasticity associated with the addition of CNTs is mild. Although the elastic response is relatively weak, it is interesting to note that the experimental evolution of G' and G'' does not follow the prediction of a single-mode Maxwell model.

A series of step strain experiments were carried out in order to reveal a more detailed relaxation behaviour of the treated CNT suspensions and to offer insights into the origin of elasticity. A finite step strain (γ_0) was applied to the CNT suspensions, and the process of stress relaxation was followed using the strain-controlled ARES rheometer. Figure 2 shows the time evolution of the relaxation modulus (G), which is defined as $G = \frac{\tau}{\gamma_0}$, for a 0.5 % CNT suspension and different values of the step strain. The stepper motor had a response time of about 0.1 s (as indicated in the figure), and for the epoxy matrix, the stress dissipated almost instantaneously consistent with the fact that it behaved essentially as a simple Newtonian fluid in both steady shear and LVE experiments. The addition of CNTs prolonged the stress relaxation process, with the CNT suspensions showing a viscoelastic response. The effect was progressive as the CNT concentration increased, and this confirmed the earlier LVE experiments that the addition of CNTs effectively increases the elasticity of the system as a whole.

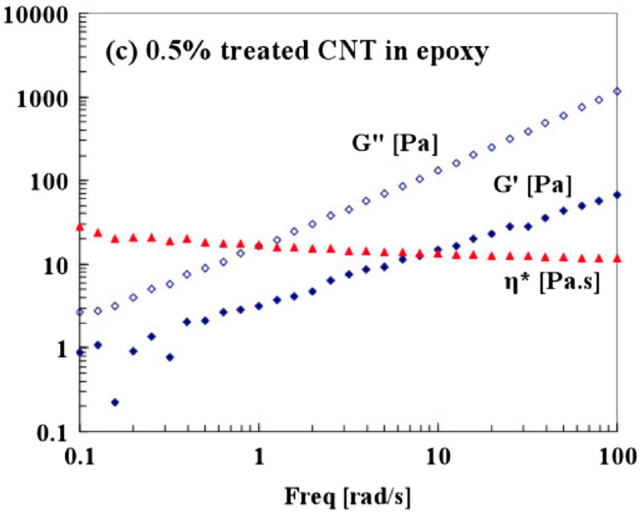

Fig. 1 Linear viscoelastic (LVE) data, which include the storage modulus (G'), the loss modulus (G'') and the complex viscosity (η^*) as a function of frequency for the 0.5 % treated CNT suspension (Ma et al. 2009)

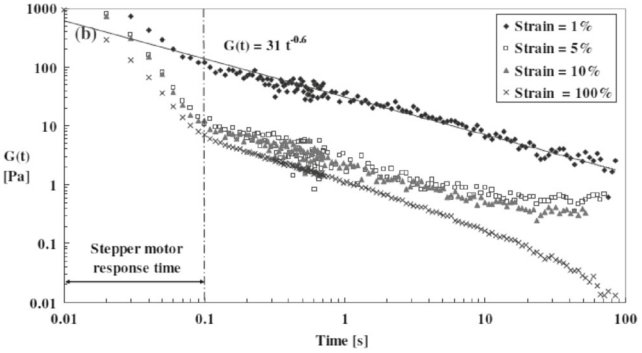

Fig. 2 Stress relaxation data for the 0.5 % CNT suspension with varying magnitudes of step strain (Ma et al. 2009)

Strains of different magnitudes were applied to the 0.5 % CNT suspension. Figure 2 shows a strain dependence in terms of the final mode of stress relaxation. At small strains (1, 5 and 10 %), the CNT suspension responded essentially as an entangled gel. At high strain, the CNT suspension behaved in a dominantly viscous fluid manner. Intuitively, the strain-dependence relaxation process can be explained by yielding a network (Amari and Watanabe 1980; Mewis and Meire 1984). Depending on the strength of the network, if a large enough strain is applied, the network will be broken down and will finally dissipate as a fluid. The network for the 0.5 % suspension is considered to be a relatively weak one, and it broke down at a strain level higher than 10 %. These findings have two implications. Firstly, it is highly probable that the mild elasticity observed in LVE measurements is linked to the presence of a weak CNT network. Secondly, the effect of elasticity is negligible at a high strain level, in line with the non-linear experiments reported in Ma et al. (2009) that revealed small diffusion effects attributed to Brownian effects and tube-tube hydrodynamic interactions.

Standard modelling

A standard modelling study was carried out in the study of Ma et al. (2009) by considering Brownian suspensions involving rods (ellipsoids of infinite aspect ratio). The main ingredients of the model are summarized in this section. For a more detailed discussion of the multiscale modelling of non-Brownian and Brownian suspensions of rods, see Chinesta (2013).

The extra-stress tensor of the suspension is given by

$$\tau = 2\eta\mathbf{D} + 2\eta N_{\mathrm{p}}\,(\mathbf{D} : \mathbf{A}) + \beta D_r \left(\mathbf{a} - \frac{\mathbf{I}}{d}\right) \tag{1}$$

where η is the viscosity of the suspending fluid (epoxy resin), $\mathbf{D}$ is the rate of strain tensor (symmetric part of the velocity gradient tensor $\nabla\mathbf{v}$), N_{p} is the particle number

that depends on the rod concentration, and $\mathbf{a}$ and $\mathbf{A}$ are the second- and fourth-order orientation tensors, respectively, defined as (Advani and Tucker 1987)

$$\mathbf{a}(\mathbf{x},t) = \int_{\mathcal{S}} \mathbf{p}\otimes\mathbf{p}\,\psi(\mathbf{x},t,\mathbf{p})\,d\mathbf{p} \tag{2}$$

and

$$\mathbf{A}(\mathbf{x},t) = \int_{\mathcal{S}} \mathbf{p}\otimes\mathbf{p}\otimes\mathbf{p}\otimes\mathbf{p}\,\psi(\mathbf{x},t,\mathbf{p})\,d\mathbf{p} \tag{3}$$

where the unit vector $\mathbf{p}$ defines the rod orientation, $\mathcal{S}$ is the surface of the unit ball, and $\psi(\mathbf{x},t,\mathbf{p})$ is the orientation distribution function that gives the fraction of rods that at position $\mathbf{x}$ and time t, are aligned along the direction $\mathbf{p}$; D_r is the diffusion coefficient, β is the parameter affecting the diffusion term, $\mathbf{I}$ is the unit tensor, and d is the dimension of physical space ($d = 2$ or 3).

The evolution equation for the second-order orientation tensor was derived in detail in the study of Chinesta (2013)

$$\dot{\mathbf{a}} = \nabla\mathbf{v}\cdot\mathbf{a} + \mathbf{a}\cdot(\nabla\mathbf{v})^T - 2\mathbf{A}:\mathbf{D} - 2dD_r\left(\mathbf{a} - \frac{\mathbf{I}}{d}\right). \tag{4}$$

In order to close the model, a suitable closure relation expressing $\mathbf{A}$ as the function of $\mathbf{a}$ is needed. Among the numerous available closure relations (Dupret and Verleye 1999; Kroger et al. 2008), we consider in what follows the linear closure relation that becomes exact for an isotropic distribution function (Advani and Tucker 1990).

LVE modelling

As LVE involves a small-amplitude oscillation applied to an essentially isotropic suspension ($\mathbf{a}^{\text{iso}} \approx \frac{\mathbf{I}}{3}$), the linear closure relation is expected to be an accurate approximation for describing $\mathbf{A}$. The linear closure reads (Advani and Tucker 1990):

$$\begin{aligned}\mathbf{A}^{lin}_{ijkl}(\mathbf{a}) = &-\frac{1}{35}\left(\mathbf{I}_{ij}\mathbf{I}_{kl} + \mathbf{I}_{ik}\mathbf{I}_{jl} + \mathbf{I}_{il}\mathbf{I}_{jk}\right)\\ &+\frac{1}{7}\left(\mathbf{a}_{ij}\mathbf{I}_{kl} + \mathbf{a}_{ik}\mathbf{I}_{jl} + \mathbf{a}_{il}\mathbf{I}_{jk} + \mathbf{a}_{kl}\mathbf{I}_{ij}\right.\\ &\left.+\mathbf{a}_{jl}\mathbf{I}_{ik} + \mathbf{a}_{jk}\mathbf{I}_{il}\right).\end{aligned} \tag{5}$$

To predict the shear stress τ_{12}, we need to compute the component $(\mathbf{A}:\mathbf{a})_{12}$ as well as the component $\mathbf{a}_{12}$ involved in the diffusion term of Eq. 1. Taking into account that the applied flow (small-amplitude oscillation) implies the strain rate

$$\mathbf{D} = \begin{pmatrix} 0 & \frac{\dot\gamma}{2} & 0\\ \frac{\dot\gamma}{2} & 0 & 0\\ 0 & 0 & 0\end{pmatrix} \tag{6}$$

and that it only induces a small perturbation of the isotropic orientation state

$$\mathbf{a}^{\text{iso}} = \begin{pmatrix} \frac{1}{3} & 0 & 0\\ 0 & \frac{1}{3} & 0\\ 0 & 0 & \frac{1}{3}\end{pmatrix}, \tag{7}$$

the linear closure approximation (5) yields $(\mathbf{A}:\mathbf{D})_{12} \approx (\mathbf{A}^{lin}(\mathbf{a}^{\text{iso}}):\mathbf{D})_{12} = \frac{\dot\gamma}{15}$.

Thus, the shear stress can be approximated in the general 3D case by

$$\tau_{12} \approx \eta\dot\gamma + \frac{2}{15}\eta N_{\text{p}}\dot\gamma + \beta D_r\mathbf{a}_{12} \tag{8}$$

wherein we can identify a viscous component (the one affected by $\dot\gamma$) and an elastic one (the one that does not depend on $\dot\gamma$). Obviously, elastic effects will be associated to the last contribution that in fact corresponds to diffusion effects that depend linearly on component $\mathbf{a}_{12}$. In order to evaluate the time evolution of $\mathbf{a}_{12}$, we consider (4) in the general 3D case ($d = 3$):

$$\dot{\mathbf{a}} = \nabla\mathbf{v}\cdot\mathbf{a} + \mathbf{a}\cdot(\nabla\mathbf{v})^T - 2\cdot\mathbf{A}:\mathbf{D} - 6D_r\left(\mathbf{a} - \frac{\mathbf{I}}{3}\right). \tag{9}$$

Now, using the same approximations as in the previous paragraphs, we obtain $(\nabla\mathbf{v}\cdot\mathbf{a}+\mathbf{a}\cdot(\nabla\mathbf{v})^T - 2\cdot\mathbf{A}:\mathbf{D})_{12} \approx \frac{\dot\gamma}{5}$. Thus, (9) reduces to

$$\dot{\mathbf{a}}_{12} \approx \frac{\dot\gamma}{5} - 6D_r\mathbf{a}_{12}. \tag{10}$$

For the sake of notational simplicity, we define $\mathbf{a}_{12} \equiv a$ and $\tau_{12} \equiv \tau$. Thus, the LVE model reads

$$\begin{cases}\tau \approx \eta\dot\gamma + \frac{2}{15}\eta N_{\text{p}}\dot\gamma + \beta D_r a\\ \dot a \approx \frac{\dot\gamma}{5} - 6D_r a\end{cases}. \tag{11}$$

Now, let us apply the small-amplitude oscillation $\gamma(t)$ given by

$$\gamma = \gamma_0 e^{i\omega t}, \tag{12}$$

with $i = \sqrt{-1}$, which results in the shear rate

$$\dot\gamma = i\omega\gamma_0 e^{i\omega t}. \tag{13}$$

From the second equation in Eq. 11, we can expect that $a(t)$ has the same oscillation frequency, but with a certain phase delay (φ), that is

$$a = a_0 e^{i\omega t - i\varphi} = \tilde a_0 e^{i\omega t}. \tag{14}$$

Introducing expressions (13) and (14) into the second equation in Eq. 11 and using the notations of Ma et al. (2009), $\lambda = \frac{1}{6D_r}$ and $\mu = \frac{1}{30D_r}$, we obtain

$$i\omega\lambda\tilde a_0 + \tilde a_0 = i\omega\mu\gamma_0, \tag{15}$$

from which we have

$$\tilde{a}_0 = \left(\frac{\lambda\mu\omega^2}{1+\lambda^2\omega^2} + i\frac{\mu\omega}{1+\lambda^2\omega^2} \right) \gamma_0. \tag{16}$$

With this result, we go back to the stress expression (first equation in Eq. 11) and write the complex stress amplitude according to

$$\begin{aligned} \tilde{\tau} = \gamma_0 \Big(& i\omega\eta \left(1 + \tfrac{2}{15} N_\mathrm{p}\right) \\ & + \beta D_r \left(\tfrac{\lambda\mu\omega^2}{1+\lambda^2\omega^2} + i\tfrac{\mu\omega}{1+\lambda^2\omega^2} \right) \Big), \end{aligned} \tag{17}$$

from which we can identify the storage and loss moduli,

$$\begin{cases} G' = \frac{\Re(\tilde{\tau})}{\gamma_0} \\ G'' = \frac{\Im(\tilde{\tau})}{\gamma_0} \end{cases}, \tag{18}$$

where $\Re(\tilde{\tau})$ and $\Im(\tilde{\tau})$ denote the real and imaginary part of $\tilde{\tau}$, respectively. We obtain

$$G' = \beta D_r \frac{\lambda\mu\omega^2}{1+\lambda^2\omega^2}, \tag{19}$$

and

$$G'' = \omega\eta \left(1 + \frac{2}{15} N_\mathrm{p}\right) + \beta D_r \frac{\mu\omega}{1+\lambda^2\omega^2}. \tag{20}$$

Thus, the loss modulus scales linearly with the frequency (ω) of the applied oscillation in agreement with the experimental findings.

The storage modulus (G') scales at small frequencies with the square ω^2 of the applied frequency. This result, however, is inconsistent with the experimental findings reported in Ma et al. (2009). See Fig. 1, wherein the storage modulus is observed to scale roughly as $\omega^{0.6}$.

In Eq. 19, we notice that D_r appears at the power -1 as both μ and λ are proportional to D_r^{-1}. Thus, by assuming that D_r is proportional to an adequate power (p) of the applied frequency (ω), i.e. $D_r \propto \omega^p$, one could control the fitting process. This was the route considered in Ma et al. (2009). It is important, however, to emphasize that this route implies a certain inconsistency: assuming a frequency-dependent diffusion coefficient implies a non-linear behaviour, while the entire analysis is based on a linearity assumption. The authors followed this route in the study of Ma et al. (2009) to avoid the introduction of many relaxation modes.

These relaxation modes could be associated with polydispersity, with thermally activated bending or flow-induced bending in the case of non-straight CNTs as proposed by Cruz et al. (2010) and (2012). In absence of the required information, however, the use of multiple modes reduces to the simple identification of the associated parameters.

In the "Fractional modelling" section, we propose an alternative, consistent and physically supported approach based on the concept of fractional derivatives.

Step strain modelling

After applying the step strain, the stress relaxation results from Eq. 1, assuming the fluid at rest

$$\tau = \beta D_r a, \tag{21}$$

were again $\tau = \tau_{12}$ and $a = \mathbf{a}_{12}$. The evolution of a can be calculated from Eq. 4 that, in the absence of flow, reduces to

$$\frac{da}{dt} = -6D_r a. \tag{22}$$

This yields an exponential decay for a and, consequently, the same decay for the shear stress τ. As discussed in the study of Ma et al. (2009), the predicted exponential decay does not agree with the power-law behaviour observed experimentally.

Fractional modelling

In complex fluids, micro-rheological experiments often exhibit anomalous sub-diffusion or sticky diffusion, in which the mean square displacement of Brownian tracer particles is found to scale as $\langle x^2 \rangle \propto t^\alpha$ with $0 < \alpha < 1$ (see Jaishankar and McKinley (2012) and the references therein). In these cases, the use of non-integer derivatives can constitute an appealing alternative as it allows one to correctly reproduce the observed physical behaviour while keeping the model as simple as possible. Moreover, from a physical point of view, the use of non-integer derivatives introduces a degree of non-locality that seems in agreement with the intrinsic nature of the physical system.

In the case of semi-diluted and semi-concentrated suspensions of functionalized CNTs, the chemical treatment creates a weakly interconnected network of CNTs responsible for the mild elasticity observed experimentally. In such a percolated system, the Brownian motion is expected to be disturbed and to exhibit anomalous diffusion.

It is well known that standard diffusion mechanisms imply a Brownian velocity

$$\dot{\mathbf{p}}|^B = -D_r \frac{\frac{\partial \psi}{\partial \mathbf{p}}}{\psi} \tag{23}$$

that leads to the equations considered in the previous section.

A fractional counterpart consists in generalizing (23) by assuming a non-integer time derivative

$$\left. \frac{d^\alpha \mathbf{p}}{dt^\alpha} \right|^B = -D_r \frac{\frac{\partial \psi}{\partial \mathbf{p}}}{\psi} \tag{24}$$

where one could expect from the experimental data that $\alpha < 1$. See Appendix A for additional information on fractional derivatives.

Now, in view (2), the time derivative of the second-order orientation tensor $\mathbf{a}$ reads

$$\frac{d\mathbf{a}}{dt} = \int_{\mathcal{S}} (\dot{\mathbf{p}} \otimes \mathbf{p} + \mathbf{p} \otimes \dot{\mathbf{p}})\ \psi\ d\mathbf{p}. \tag{25}$$

Here, the effective rotary velocity $\dot{\mathbf{p}}$ is given by

$$\dot{\mathbf{p}} = \dot{\mathbf{p}}|^J + \dot{\mathbf{p}}|^B \tag{26}$$

where $\dot{\mathbf{p}}|^J$ is the flow-induced velocity expressed from Jeffery's equation (Jeffery 1922; Chinesta 2013)

$$\dot{\mathbf{p}}|^J = \nabla\mathbf{v} \cdot \mathbf{p} - (\nabla\mathbf{v} : (\mathbf{p} \otimes \mathbf{p}))\, \mathbf{p}, \tag{27}$$

and $\dot{\mathbf{p}}|^B$ is the velocity related to fractional diffusion

$$\dot{\mathbf{p}}|^B = -D_r \frac{d^{1-\alpha}}{dt^{1-\alpha}} \left(\frac{d^\alpha \mathbf{p}}{dt^\alpha}\bigg|^B \right) = -D_r \frac{d^{1-\alpha}}{dt^{1-\alpha}} \left(\frac{\frac{\partial \psi}{\partial \mathbf{p}}}{\psi} \right). \tag{28}$$

Introducing the effective rotary velocity into Eq. 25 and proceeding as described in Appendix B, we obtain

$$\frac{d\mathbf{a}}{dt} = \dot{\mathbf{a}}|^J - 6D_r \frac{d^{1-\alpha}}{dt^{1-\alpha}} \left(\mathbf{a} - \frac{\mathbf{I}}{3} \right) \tag{29}$$

with $\dot{\mathbf{a}}|^J = \nabla\mathbf{v} \cdot \mathbf{a} + \mathbf{a} \cdot (\nabla\mathbf{v})^T - 2(\mathbf{A} : \nabla\mathbf{v})$.

LVE fractional model

Since the extra-stress tensor of the suspension is given by

$$\tau = 2\eta\mathbf{D} + 2\eta N_\mathrm{p} (\mathbf{D} : \mathbf{A}) + \beta D_r \left(\mathbf{a} - \frac{\mathbf{I}}{3} \right) \tag{30}$$

and using again the linear closure and the same rationale as in the "Standard modelling" section, we obtain

$$\tau_{12} \approx \eta\dot{\gamma} + \frac{2}{15}\eta N_\mathrm{p}\dot{\gamma} + \beta D_r \mathbf{a}_{12}. \tag{31}$$

On the other hand, the orientation evolution equation reads

$$\dot{\mathbf{a}} = \nabla\mathbf{v}\cdot\mathbf{a} + \mathbf{a}\cdot(\nabla\mathbf{v})^T - 2\mathbf{A} : \mathbf{D} - 6D_r \frac{d^{1-\alpha}}{dt^{1-\alpha}} \left(\mathbf{a} - \frac{\mathbf{I}}{3} \right). \tag{32}$$

With the notations $\mathbf{a}_{12} \equiv a$ and $\tau_{12} \equiv \tau$, the LVE fractional model thus yields

$$\begin{cases} \tau \approx \eta\dot{\gamma} + \frac{2}{15}\eta N_\mathrm{p}\dot{\gamma} + \beta D_r a \\ \frac{da}{dt} \approx \frac{\dot{\gamma}}{5} - 6D_r \frac{d^{1-\alpha}a}{dt^{1-\alpha}} \end{cases}. \tag{33}$$

As in the "LVE modelling" section, we apply the small-amplitude oscillation $\gamma(t) = \gamma_0 e^{i\omega t}$. From the second equation in Eq. 33, we expect that $a(t)$ has the same oscillation frequency, but with a certain phase delay (φ), that is

$$a = a_0 e^{i\omega t - i\varphi} = \tilde{a}_0 e^{i\omega t}. \tag{34}$$

With the notations $\lambda = \frac{1}{6D_r}$ and $\mu = \frac{1}{30D_r}$, we obtain

$$i\omega\lambda\tilde{a}_0 + (i\omega)^{1-\alpha}\tilde{a}_0 = i\omega\mu\gamma_0 \tag{35}$$

where $i^{1-\alpha} = \chi + i\nu$, with $\chi^2 + \nu^2 = 1$. Thus, Eq. 35 can be rewritten as

$$i\omega\lambda\tilde{a}_0 + (\chi + i\nu)\omega^{1-\alpha}\tilde{a}_0 = i\omega\mu\gamma_0, \tag{36}$$

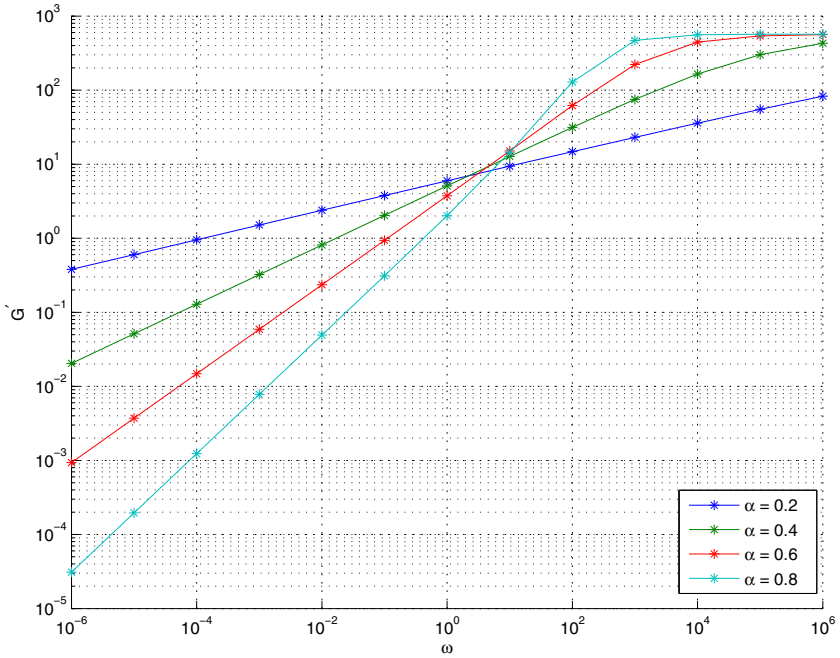

Fig. 3 LVE storage modulus for different values of the derivative order ($D_r = 15$ and $\beta = 190$)

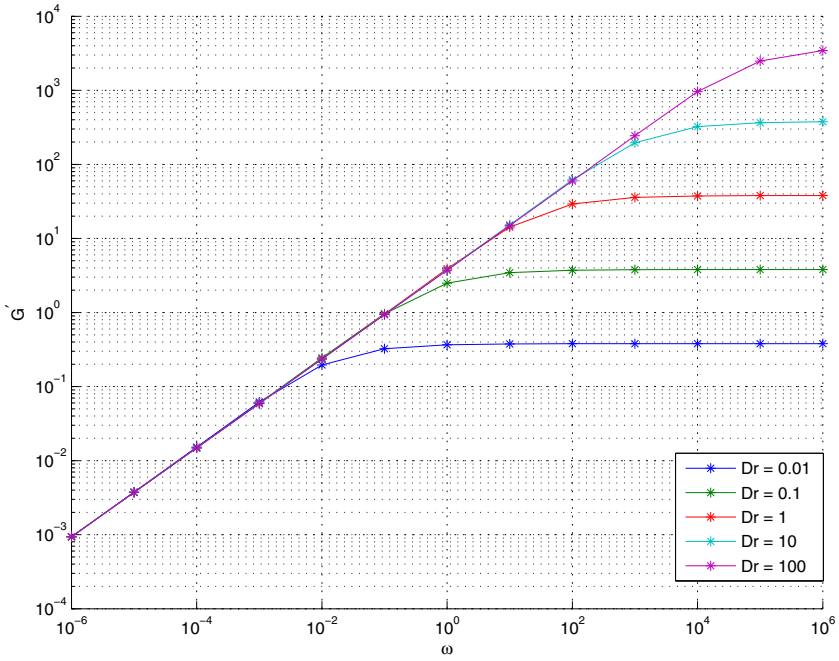

Fig. 4 LVE storage modulus for different values of the diffusion coefficient (D_r) ($\alpha = 0.6$ and $\beta = 190$)

from which we have

$$\tilde{a}_0 = \gamma_0 \left(\frac{\lambda\mu\omega^2 + \mu\nu\omega^{2-\alpha}}{\chi^2\omega^{2(1-\alpha)} + (\omega\lambda + \nu\omega^{1-\alpha})^2} + i\frac{\mu\chi\omega^{2-\alpha}}{\chi^2\omega^{2(1-\alpha)} + (\omega\lambda + \nu\omega^{1-\alpha})^2} \right). \tag{37}$$

Note that for the case of the integer model $\alpha = 1$, we have $\chi = 1$ and $\nu = 0$, and the previous expression reduces to the one considered in the "Standard modelling" section.

From Eq. 37, we go back to the stress expression (first equation in Eq. 33) and write the complex stress amplitude according to

$$\tilde{\tau} = \gamma_0 \left(i\omega\eta \left(1 + \frac{2}{15} N_p \right) + \beta D_r \left(\frac{\lambda\mu\omega^2 + \mu\nu\omega^{2-\alpha}}{\chi^2\omega^{2(1-\alpha)} + (\omega\lambda + \nu\omega^{1-\alpha})^2} + i\frac{\mu\chi\omega^{2-\alpha}}{\chi^2\omega^{2(1-\alpha)} + (\omega\lambda + \nu\omega^{1-\alpha})^2} \right) \right), \tag{38}$$

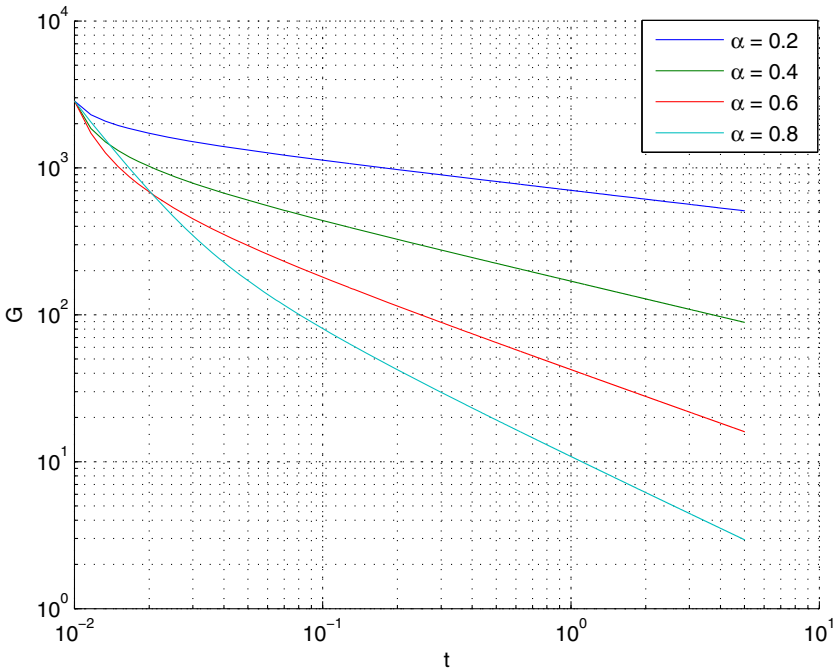

Fig. 5 Step strain modulus for different values of the derivative order ($D_r = 15$ and $\beta = 190$)

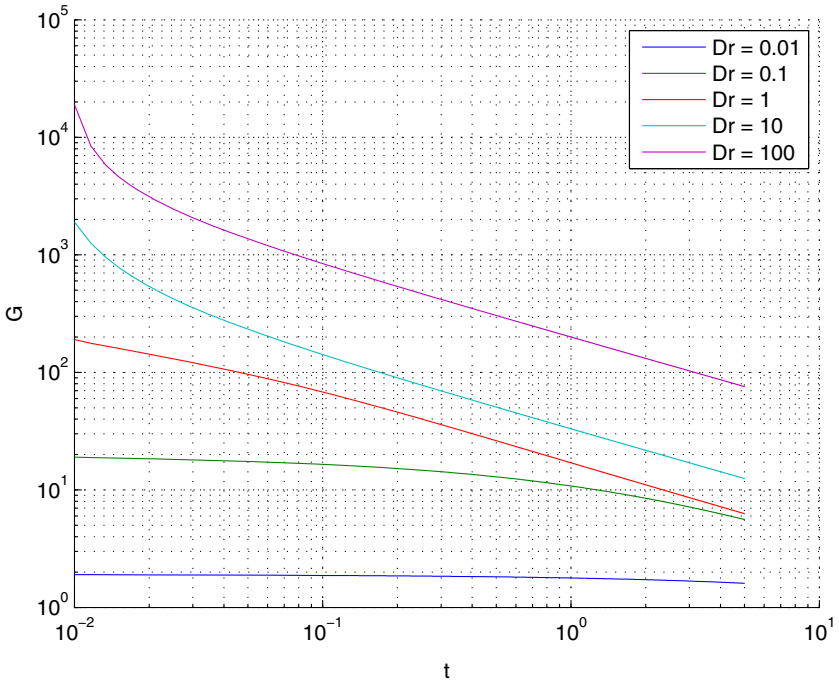

Fig. 6 Step strain modulus for different values of the diffusion coefficient (D_r) ($\alpha = 0.6$ and $\beta = 190$)

from which we identify the storage modulus,

$$G' = \beta D_r \frac{\lambda\mu\omega^2 + \mu\nu\omega^{2-\alpha}}{\chi^2\omega^{2(1-\alpha)} + (\omega\lambda + \nu\omega^{1-\alpha})^2}, \tag{39}$$

and the loss modulus,

$$G'' = \omega\eta\left(1 + \frac{2}{15}N_p\right) + \beta D_r \frac{\mu\chi\omega^{2-\alpha}}{\chi^2\omega^{2(1-\alpha)} + (\omega\lambda + \nu\omega^{1-\alpha})^2}. \tag{40}$$

At small frequencies, the predicted storage modulus (G') scales as ω^α, i.e. with the power α of the applied frequency. Thus, it suffices to select $\alpha = 0.6$ to describe the observed experimental behaviour in the framework of a consistent linear and single-mode theory.

Step strain fractional model

As in the "Step strain modelling" section, the stress relaxation after a step strain is given by

$$\tau = \beta D_r a \tag{41}$$

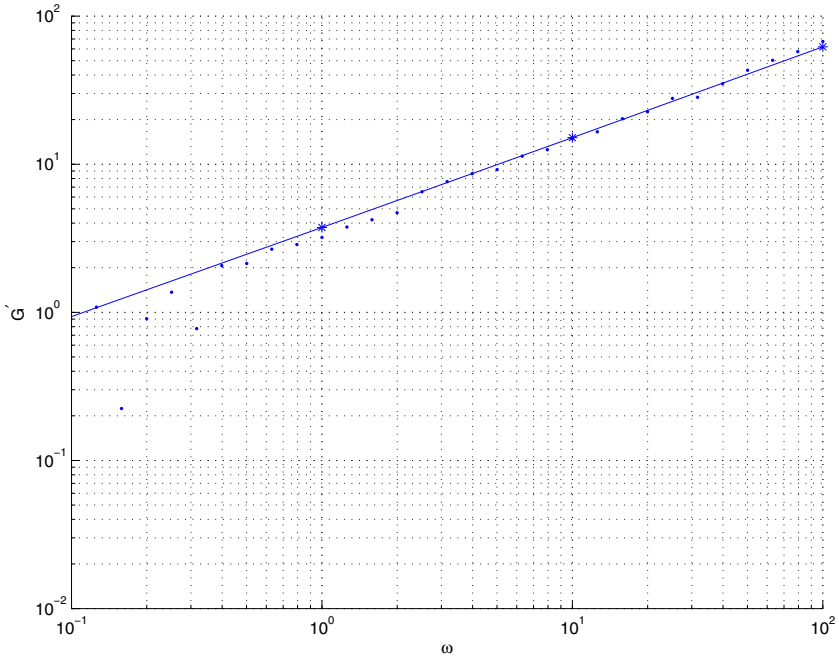

Fig. 7 LVE storage modulus. Prediction of the fractional model ($\alpha = 0.6$, $D_r = 15$ and $\beta = 190$) versus experimental data

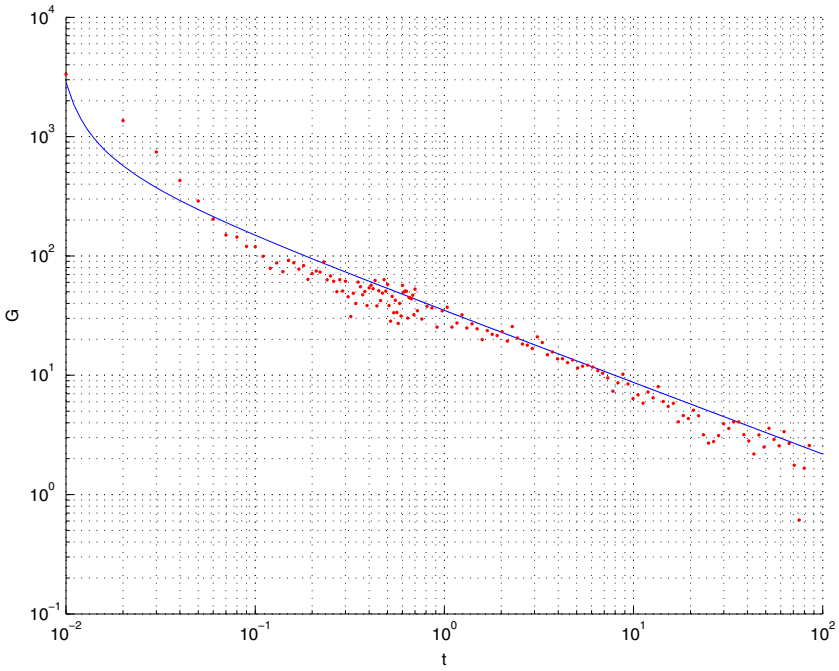

Fig. 8 Step strain modulus. Prediction of the fractional model ($\alpha = 0.6$, $D_r = 15$ and $\beta = 190$) versus experimental data

where the evolution of a is now calculated from

$$\frac{da}{dt} = -6D_r \frac{da^{1-\alpha}}{dt^{1-\alpha}}, \tag{42}$$

instead of using the standard integer model (22). The numerical solution of Eq. 42 injected into Eq. 41 yields a prediction of stress relaxation.

As shown in the next section, the use of the fractional model indeed leads to a power-law behaviour in agreement with the experimental findings.

Fractional model predictions versus experimental data

In what follows, we discuss predictions of the proposed fractional model in terms of the LVE storage modulus (G') and the step strain modulus (G).

The fractional model has three parameters: (i) the derivative order (α), (ii) the diffusion coefficient (D_r) and (iii) the parameter (β) that quantifies the stress response.

The derivative order (α) can be identified easily as it determines the slopes of G' and G. The coefficients D_r and β are adjusted to fit the experimental data.

Figures 3 and 4 depict the global behaviour of the storage modulus for different values of the derivative order (α) and the diffusion coefficient (D_r), respectively. Figures 5 and 6 depict similar predictions for the time evolution of G in step strain.

Finally, the fractional model fitting of LVE and step strain experimental data was performed by considering $\alpha = 0.6$, $D_r = 15$ and $\beta = 190$. Figures 7 and 8 depict the fit for the storage modulus and the step strain relaxation, respectively. An excellent agreement is obtained, giving us confidence as to the relevance of the proposed fractional model.

Conclusions

We have revisited in this paper the rheological modelling of chemically treated CNT suspensions, first addressed in the study of Ma et al. (2009). It was noticed in LVE experiments that such suspensions exhibit mild elasticity characterized by storage modulus scaling with the power 0.6 of the applied frequency.

The elasticity resulting from the standard Brownian rotary diffusion is unable to match these experimental data by considering a single-mode model. Obviously, one possibility consists in introducing a spectrum of relaxation times able to fit available data, but such an approach is difficult to support physically.

Many authors noticed the existence of anomalous diffusion mechanisms and proposed to model these phenomena by means of models involving fractional (non-integer) derivatives. In this work, we followed a similar route for modelling the LVE and step strain behaviour of chemically treated CNT suspensions. We have shown that a single-mode fractional derivative description of rotary diffusion with a derivative order ($\alpha = 0.6$) suffices for describing the available experimental data.

Appendix A: On fractional derivatives

There are many books on fractional calculus and fractional differential equations (e.g. Kilbas et al. 2006; Podlubny 1999). We summarize here the main concepts needed to understand the developments carried out in this paper.

We start with the formula usually attributed to Cauchy for evaluating the nth integration, $n \in \mathbb{N}$, of a function $f(t)$

$$J^n f(t) := \int \cdots \int_0^t f(\tau)\, d\tau = \frac{1}{(n-1)!}\int_0^t (t-\tau)^{n-1} f(\tau)\, d\tau. \quad (43)$$

This can be rewritten as

$$J^n f(t) = \frac{1}{\Gamma(n)}\int_0^t (t-\tau)^{n-1} f(\tau)\, d\tau \quad (44)$$

where $\Gamma(n) = (n-1)!$ is the gamma function. In the latter being in fact defined for any real value $\alpha \in \mathbb{R}$, we can define the fractional integral from

$$J^\alpha f(t) := \frac{1}{\Gamma(\alpha)}\int_0^t (t-\tau)^{\alpha-1} f(\tau)\, d\tau. \quad (45)$$

Now, if we consider the fractional derivative order (α), we seect an integer $m \in \mathbb{N}$ such that $m-1 < \alpha < m$, and it suffices to consider an integer m-order derivative combined with a $(m-\alpha)$ fractional integral. Obviously, we could take the derivative of the integral or the integral of the derivative, resulting in the left- and right-hand definitions of the fractional derivative usually denoted by $D^\alpha f(t)$ and $D^\alpha_* f(t)$, respectively.

Because these approaches to the fractional derivative began with an expression for the repeated integration of a function, one could consider a similar approach for the derivative. This was the route considered by Grunwald and Letnikov (GL) that defined the so-called 'differintegral' that leads to the fractional counterpart of the usual finite differences. In the present work, we use the GL definition of the fractional derivative.

It turns out that the composition of fractional derivatives follows a rule similar to that for standard derivatives. On the other hand, the Fourier transform of a fractional derivative of order α reads $\mathcal{F}(g(t);\omega) = (i\omega)^\alpha \mathcal{G}(\omega)$. This property is particularly useful when addressing harmonic responses as in the case of LVE experiments.

Appendix B: Derivation of the fractional derivative of the orientation tensor

We discuss the contribution of fractional diffusion to the rod rotary velocity (the flow-induced contribution remains unchanged)

$$\left.\frac{d^\alpha \mathbf{p}}{dt^\alpha}\right|^B = -D_r \frac{\frac{\partial \psi}{\partial \mathbf{p}}}{\psi}. \quad (46)$$

Now, we consider the second-order orientation tensor

$$\mathbf{a} = \int_{\mathcal{S}} \mathbf{p}\otimes\mathbf{p}\ \psi\ d\mathbf{p} \quad (47)$$

whose time derivative can be rewritten as

$$\dot{\mathbf{a}}|^B = \frac{d^{1-\alpha}}{d^{1-\alpha}}\left\{\frac{d^\alpha}{dt^\alpha}\left\{\int_{\mathcal{S}} (\mathbf{p}\otimes\mathbf{p}+\mathbf{p}\otimes\mathbf{p})\ \psi\ d\mathbf{p}\right\}\right\} \quad (48)$$

or

$$\dot{\mathbf{a}}|^B = \frac{d^{1-\alpha}}{d^{1-\alpha}}\left\{\int_{\mathcal{S}} \frac{d^\alpha}{dt^\alpha}(\mathbf{p}\otimes\mathbf{p}+\mathbf{p}\otimes\mathbf{p})\ \psi\ d\mathbf{p}\right\}. \quad (49)$$

Considering the first term of Leibnitz's rule related to the fractional derivative of a product of functions (it is easy to prove that the second one leads to the standard diffusion integer term, while the others can be neglected), we obtain

$$\dot{\mathbf{a}}|^B \approx \frac{d^{1-\alpha}}{d^{1-\alpha}}\left\{\int_{\mathcal{S}} \left(\frac{d^\alpha \mathbf{p}}{dt^\alpha}\otimes\mathbf{p}+\mathbf{p}\otimes\frac{d^\alpha\mathbf{p}}{dt^\alpha}\right)\psi\ d\mathbf{p}\right\} \quad (50)$$

or

$$\dot{\mathbf{a}}|^B \approx -D_r \frac{d^{1-\alpha}}{d^{1-\alpha}}\left\{\int_{\mathcal{S}} \left(\frac{\frac{\partial\psi}{\partial\mathbf{p}}}{\psi}\otimes\mathbf{p}+\mathbf{p}\otimes\frac{\frac{\partial\psi}{\partial\mathbf{p}}}{\psi}\right)\psi\ d\mathbf{p}\right\}, \quad (51)$$

which finally gives

$$\dot{\mathbf{a}}|^B \approx -2dD_r \frac{d^{1-\alpha}}{d^{1-\alpha}}\left(\mathbf{a}-\frac{\mathbf{I}}{d}\right). \quad (52)$$

References

Abisset-Chavanne E, Mezher R, Le Corre S, Ammar A, Chinesta F (2013) Kinetic theory microstructure modeling in concentrated suspensions. Entropy 15:2805–2832. doi:10.3390/e15072805

Abisset-Chavanne E, Chinesta F, Ferec J, Ausias G, Keunings, R (2014) On the multiscale description of dilute suspensions of non-Brownian rigid clusters composed of rods. J Non-Newtonian Fluid Mech. doi:10.1016/j.jnnfm.2014.08.014

Advani S, Tucker CL (1987) The use of tensors to describe and predict fiber orientation in short fiber composites. J Rheol 31:751–784

Advani S, Tucker CL (1990) Closure approximations for three-dimensional structure tensors. J Rheol 34:367–386

Amari T, Watanabe K (1980) Stress relaxation of carbon black-linseed oil suspensions. J Soc Rheol Jpn 8:80-83

Carter LF (1967) A study of the rheology of suspensions of rod-shaped particles in a Navier-Stokes liquid. Ph.D. dissertation, University of Michigan, Ann Arbor

Chinesta F (2013) From single-scale to two-scales kinetic theory descriptions of rods suspensions. Arch Comput Methods Eng 20:1–29

Cueto E, Ma AWK, Chinesta F, Mackley MR (2008) Numerical simulation of spin coating processes involving functionalised carbon nanotube suspensions. Int J Mater Form 1:89–99

Cueto E, Monge R, Chinesta F, Poitou A, Alfaro I, Mackley MR (2010) Rheological modeling and forming process simulation of CNT nanocomposites. Int J Mater Form 3:1327–1338

Cruz C, Illoul L, Chinesta F, Regnier G (2010) Effects of a bent structure on the linear viscoelastic response of carbon nanotube diluted suspensions. Rheologica Acta 49:1141–1155

Cruz C, Chinesta F, Regnier G (2012) Review on the Brownian dynamics simulation of bead-rod-spring models encountered in computational rheology. Arch Comput Methods Eng 19/2:227–259

Dupret F, Verleye V (1999) Modelling the flow of fibre suspensions in narrow gaps. In: Siginer DA, De Kee D, Chabra RP (eds) Advances in the flow and rheology of non-newtonian fluids, rheology series. Elsevier, pp 1347–1398

Ganani E, Powell RL (1986) Rheological properties of rodlike particles in a Newtonian and non-Newtonian fluid. J Rheol 30:995–1013

Jaishankar A, McKinley GH (2012) Power-law rheology in the bulk and at the interface: quasi-properties and fractional constitutive equations. Proc R Soc. doi:10.1098/rspa.2012.0284

Jeffery GB (1922) The motion of ellipsoidal particles immersed in a viscous fluid. Proc R Soc London A102:161–179

Kilbas A, Srivastava HM, Trujillo JJ (2006) Theory and applications of fractional differential equations. Elsevier

Kroger M, Ammar A, Chinesta F (2008) Consistent closure schemes for statistical models of anisotropic fluids. J Non-Newtonian Fluid Mech 149:40–55

Ma A, Chinesta F, Mackley MR, Ammar A (2008) The rheological modelling of carbon nanotube (CNT) suspensions in steady shear flows. Int J Mater Form 2:83–88

Ma A, Chinesta F, Ammar A, Mackley MR (2008) Rheological modelling of carbon nanotube aggregate suspensions. J Rheol 52/6:1311–1330

Ma A, Chinesta F, Mackley MR (2009) The rheology and modelling of chemically treated carbon nanotube suspensions. J Rheol 53/3:547–573

Mewis J, Meire C (1984) Yielding in weakly flocculated systems. In: Mena B, Garcia-Rejon A, Rangel-Nafaille C (eds) Advances in rheology, volume 2: fluids. Elsevier

Podlubny I (1999) Fractional differential equations. Academic, San Diego

Rahatekar SS, Koziol KK, Butler SA, Elliott JA, Shaffer MSP, Mackley, MR, Windle AH (2006) Optical microstructure and viscosity enhancement for an epoxy resin matrix containing multiwall carbon nanotubes. J Rheol 50:599–610

Song YK, Youn JR (2005) Influence of dispersion states of Carbon Nanotubes on physical properties of epoxy nanocomposites. Carbon 43:1378–1385

Xu JS, Chatterjee S, Koelling KW, Wang Y, Bechtel SE (2005) Shear and extensional rheology of carbon nanofibers suspensions. Rheol Acta 44:537–562

Yearsley KM, Mackley MR, Chinesta F, Leygue A (2012) The rheology of multiwalled carbon nanotube and carbon black suspensions. J Rheol 56:1465–1490